Analytica Chimica Acta 1278 (2023) 341659

Contents lists available at ScienceDirect

Analytica Chimica Acta

journal homepage: www.elsevier.com/locate/aca

Simultaneous separation and detection of nine kynurenine pathway metabolites by reversed-phase liquid chromatography-mass spectrometry: Quantitation of inflammation in human cerebrospinal fluid and plasma

Vijay D. Patel [a], Shahab A. Shamsi [a,*], Andrew Miller [b], Aimin Liu [c], Mark Powell [d]

[a] Department of Chemistry, Georgia State University, Atlanta, GA, 30303, USA
[b] Department of Psychiatry and Behavioral Sciences, Emory University, Atlanta, GA, 30322, USA
[c] Department of Chemistry, The University of Texas at San Antonio, San Antonio, TX, 78249, USA
[d] Agilent Technologies, Wilmington, DE, 19808, USA

HIGHLIGHTS

- A low-cost HPLC-MS/MS method was developed using a combination of an octyl column and a ternary mobile phase for simultaneous separation and detection of all metabolites of the kynurenine pathway (KP).
- Nine KP metabolites were simultaneously separated for the first time in under 10 min.
- Method was validated for selectivity, sensitivity, and linearity as well as precision, accuracy, and matrix effect.
- We correlated neuroprotective and neurotoxic metabolite levels in CSF and plasma of low versus high inflammation subjects.

GRAPHICAL ABSTRACT

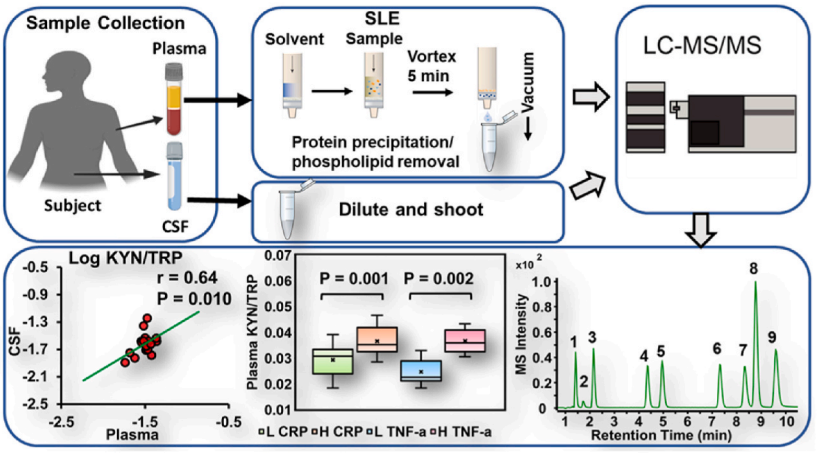

ARTICLE INFO

Keywords:
Simultaneous separation
Quantitation
Kynurenine pathway metabolites
Solid-liquid extraction
Human cerebrospinal fluid and plasma

ABSTRACT

Background: The kynurenine pathway (KP) generates eight tryptophan (TRP) metabolites collectively called kynurenines, which have gained enormous interest in clinical research. The importance of KP for different disease states calls for developing a low-cost and high-throughput chromatography-mass spectrometry method to evaluate the potential of different kynurenines. Simultaneous separation of TRP and its eight metabolites is challenging because they have substantial polarity differences (log $P = -2.5$ to $+1.3$).
Results: A low-cost, reversed-phase LC-MS/MS method based on polarity partitioning was established to simultaneously separate and quantitate all nine kynurenine pathway metabolites (KPMs) in a single run for the first time in the open literature. Based on stationary phase screening and ternary mobile phase optimization strategy, high polarity KPMs were retained while medium and low polarity KPMs were eluted in a shorter time. After

* Corresponding author. Department of Chemistry, Georgia State University, Atlanta, GA, 30303, USA.
E-mail address: sshamsi@gsu.edu (S.A. Shamsi).

https://doi.org/10.1016/j.aca.2023.341659
Received 18 April 2023; Received in revised form 24 July 2023; Accepted 25 July 2023
Available online 26 July 2023

method validation, we demonstrated the applicability of this LC/MS/MS method by quantitative measurement of all nine KPM in cerebrospinal fluid (CSF) and plasma among two groups of human subjects diagnosed with depression. Furthermore, we measured the differential KPMs in these two groups of low and high inflammation and correlated the results with CRP or TNF-α markers for depression.

Significance: Our proposed LC-MS/MS provides a new metabolite assay that can be easily applied in various clinical applications to simultaneously quantify multiple biomarkers in KP dysfunction.

1. Introduction

Tryptophan (TRP) is one of the nine essential amino acids in the human body metabolized mainly through two major pathways, serotonin, and kynurenine pathways (KP) [1]. About 90% of TRP in major organs (brain, liver, and intestine) and the peripheral system is catabolized through the KP, producing intermediate metabolites that are immunosuppressive, neurotoxic, or neuroprotective [1,2]. The enzymatic metabolism of TRP via KP suggests that the two rate-limiting enzymes, tryptophan-2,3-dioxygenase (TDO) in the liver and indoleamine-2, 3-dioxygenase (IDO) in the central nervous system, catabolizes TRP to produce kynurenine (KYN) [3]. The enzymatic breakdown of KYN produces several intermediates, of which 3-hydroxy kynurenine (3-OHKYN), 3-hydroxy anthranilic acid (3-OHAA), and quinolinic acid (QA) are neurotoxic, while kynurenic acid (KA), anthranilic acid (AA), xanthurenic acid (XA), and picolinic acid (PA) are neuroprotective (structures and log P values shown in Fig. S1) [4]. The dysregulation of TRP and intermediates such as KYN, 3-OHKYN, KA, and QA are reported in neuroinflammation, HIV, Alzheimer's disease, depression, schizophrenia, and cancer [5,6]. Because of considerable evidence of the link between disease conditions and neuroinflammation [4,7], KPMs measurements have gained enormous interest in clinical research. Recently, a new study showed depletion of TRP and dysregulation of KPMs in COVID-19 patients with mild, moderate, and severe infections [8]. The concentration levels of many KPMs, including the KYN/TRP ratio in the serum, were significantly affected in COVID infections resulting in the activation of KP [8,9]. To understand the pathophysiology of KPMs in a wide range of diseases and discover potential biomarkers for diagnostics, it is important to measure them concurrently. The challenges in the simultaneous measurement of KPM are the wide range of polarity and functional groups, a significant difference in the endogenous level, matrix effect, selectivity, and repeatability of measurements in a biospecimen. Thus, there is a need to develop a selective, sensitive, rapid, and robust method for the quantitation of all KPMs with high sample throughput.

Several methods are developed based on UV and fluorescence detection to analyze KPMs [10]. However, these methods may have shortcomings of poor sensitivity, selectivity, and specificity in complex matrices. In recent times, mass spectrometric methods have become most useful for sensitive and selective analysis of a wide range of biological samples. Especially MS/MS has proved to be one of the most sensitive, selective, and quantitative methods in bioanalysis [11]. Several methods for quantitative analysis of KPMs in biological samples using GC-MS/MS [12], CE-MS/MS [13], and HPLC-MS/MS [2,11,14] platforms have been developed. However, the simultaneous separation of all nine KPMs is still challenging for three reasons. First, the KPMs exhibit varying polarity. Four of these metabolites are very polar (e.g., QA, PA, 3-OHKYN, and KYN), whereas others are non-polar (e.g., 3-OHAA, TRP, XA, KA, and AA) and contain acidic and basic groups, resulting in different ionization in the mobile phase and chromatographic behavior. Second, in the biological matrices, the ESI may be affected and severely compromise the detection of certain KPMs. Third, marked differences in the endogenous concentrations of KPMs in biological specimens make the simultaneous quantitation challenging. For example, TRP is present in the micromolar range in the human plasma, while metabolites of TRP are present in the micro to nanomolar range [5,15,16].

Recently, our research group develop an open tubular capillary electrochromatography (CEC)-MS/MS method for the separation of all nine KP metabolites using acrylamido-2-methyl-1-propanesulfonic acid functionalized stationary phase [13]. Although the separation of six downstream metabolites was achieved in less than 30 min, the challenging simultaneous separation of all nine KP metabolites was only accomplished by increasing the column length and simultaneous application of internal pressure and voltage in 114 min. There are numerous reports on methods for HPLC-MS quantitation but only for a few KPMs [14,17–19]. For example, metabolites such as PA and QA are quantified using different methods (e.g., using separate LC columns and ESI mode for PA and QA) [18]. Also, single analysis methods using reversed-phase LC columns often require time-consuming derivatization procedures, whereas HILIC provides analysis of only a few hydrophilic KPMs but without suitable peak shapes [20]. Nevertheless, the challenge of separating TRP and its eight metabolites can be realized from the latest report in which researchers screened C-8, C-12, Phenyl-Hexyl, and seven different C-18 phases [20]. Despite these efforts, simultaneous analysis was possible only after the derivatization process, which can be tedious. Another paper on UHPLC-MS/MS method separated TRP and its metabolites in 7 min while excluding AA [21]. It should be noted that the UHPLC operation requires high quality and expensive equipment but also excessive solvent and large disposable cost of the solvent. Additionally, a skilled operator for instrument operation and maintenance is needed. There are studies on simultaneous quantitation of a few KPMs, but to the best of our knowledge, there is no report on baseline separation and quantitation of all nine underivatized KPMs in a single run on a low-cost standard HPLC-MS format.

This study proposed a robust, sensitive, highly selective, low-cost, and easy-to-operate LC-MS/MS method for simultaneous quantitation of TRP and its eight metabolites in human CSF and plasma. Four different stationary phases, namely C-8, C-18, Phenyl-Hexyl, and HILIC, were screened to compare the separation selectivity of all nine KPMs. Furthermore, the mobile phase composition and flow rates were optimized. Baseline separation of nine analytes within 10 min was achieved using a unique combination of a C-8 stationary phase and a ternary mobile phase containing acetonitrile (ACN), methanol (MeOH), and H_2O in formic acid (FA). We demonstrated the potential of this developed HPLC-MS/MS method through the simultaneous quantitation of nine KPMs in CSF and plasma (collected at times t_1 and t_2) of human subjects undergoing drug therapy for neuroinflammation (low and high). The statistical analysis showed a positive correlation between KPMs levels in human plasma, and CSF, and some of the correlations were statistically significant. The results suggest that the developed HPLC-MS/MS to simultaneously measure the levels of KPMs in different matrices is promising for biomarker discovery and clinical diagnosis. The developed method could be potentially applied to study the regulation of TRP and its eight metabolites in disease conditions to discover new biomarkers for the diagnosis of COVID-19.

2. Materials and methods

2.1. Reagents

Reference standards [picolinic acid (PA) (99%), L-kynurenine (KYN) (>98.0%), kynurenic acid (KA) (>98.0%), xanthurenic acid (XA) (>98%), methanol (MeOH) LC-MS grade (99.8%) and acetonitrile

(ACN) HPLC grade were purchased from Fischer Scientific (Hanover Park, IL, USA)]. Anthranilic acid (AA) > 98%, quinolinic acid (QA), 3-hydroxy-D, L-kynurenine (3-OHKYN) (>98%), L-tryptophan (TRP) 98%, and formic acid (>95%, were purchased from Sigma Aldrich (St. Louis, MO, USA). The 3-hydroxy anthranilic acid (3-OHAA) (>98%) was purchased from Cayman Chemicals (Ann Arbor, MI, USA). Stable isotopic-labeled (SIL) used as internal standard (IS) such as PA-D4 99.3%, QA-D3 98%, KA-D5 99.3% CDN isotopes (Pointe-Claire, Quebec, Canada), AA-15 N 98% Cambridge isotopes (Andover, MA, USA), 3-OHAA-D3, rac-3-OHKYN-13C2 15 N, DL-TRP-D8, XA-D4, L-KYN-D4 TFA salt were obtained from LGC standards (Manchester, NH, USA). Triple deionized (TDI) water was obtained from the Barnstead Nanopure II water system (Barnstead International, Dubuque, IA, USA). Phree™ Phospholipid removal cartridges were purchased from Phenomenex (Torrance, CA, USA). Eppendorf microcentrifuge tubes were purchased from Beckman Coulter (Indianapolis, IN, USA). Human plasma and CSF samples were obtained from Dr. Andrew Miller's lab (Emory University, Atlanta, GA, USA). The healthy human plasma (lyophilized solid powder containing 4% trisodium citrate as an anticoagulant) was purchased from Sigma Aldrich (St. Louis, MO, USA).

2.2. Preparation of standards, internal standards, CSF, and plasma

2.2.1. Preparation of standards and SILs stocks

All the stock solutions were prepared in the dark using the yellow light of the cell phone. Standard and internal standard (I.S) stocks were prepared in appropriate solvents according to their solubility and stability. Standard stock solutions of 3-OHKYN, 3-OHAA, TRP, and XA were prepared at 3 mM, KYN and KA were prepared at 4 mM, PA, and AA were prepared at 5 mM, and QA was prepared at 6 mM in TDI water. The stock solutions of isotopic I.S [aka. standard isotopic labels (SILs)] PA-D4, QA-D3, XA-D4, and KA-D5 were prepared at 8.0, 3.0, 3.5, and 6.0 mM, respectively, in 80/20 ACN/H2O and AA-15 N was prepared at 5.0 mM in ACN. The stock solutions of L-KYN-D4 and 3-OHKYN-13C215 N were prepared at 2.0 and 3.0 mM, respectively, in MeOH containing 0.1% (v/v) FA and 0.02% (w/v) ascorbic acid. The stock solutions of 3-OHAA-D3 and TRP-D8 were prepared at 2.0 and 3.1 mM, respectively, in 50:50 MeOH/H2O containing 0.1% (v/v) FA and 0.02% (w/v) ascorbic acid. All the standards and SILs stock solutions were stored at −20 °C, and −80 °C, respectively and were stable for at least one month.

2.2.2. Preparation of working standards and SILs

Working solutions of standards and SILs were prepared by diluting the stocks (prepared in section 1.2.1) with TDI water. The working standard mixtures A (two analytes), B (seven analytes), C (eight analytes), D (1 analyte), and SIL were prepared separately. A working standard mixture A containing 100 μM PA and 101 μM QA was prepared by aliquoting 70 μL of stock of PA and 59 μL of stock of QA and diluting to a final volume of 3.5 mL with TDI water. A working standard mixture B containing 150 μM 3-OHKYN, 151 μM KYN, 150 μM 3-OHAA, 150 μM TRP, 150 μM XA, 130 μM kA, and 152 μM AA was prepared by aliquoting 200 μL of 3-OHKYN, 3-OHAA, TRP, and XA stock solutions; 120 μL of AA, 130 μL of KA, and 150 μL of KYN stock solutions, and diluting all to a final volume of 4.0 mL with TDI water. A working standard mixture C containing 11.4 μM PA, 43 μM QA, 25.7 μM 3-OHKYN, 322.3 μM KYN, 11.1 μM 3-OHAA, 107.1 μM XA, 11.4 μM kA, and 11.4 μM AA was prepared by aliquoting 8 μL of PA, 25 μL of QA, 30 μL of 3-OHKYN, 282 μL of KYN, 13 μL 3-OHAA, 125 μL of XA, 10 μL of KA, and 8 μL of AA stock solutions and diluting to a final volume of 3.5 mL with TDI water. The working standard mixture D containing 150 μM TRP was prepared by aliquoting 240 μL of TRP stock solution and diluting to the final volume of 2.5 mL TDI water. Working SIL-A mixture consisted of PA-D4, 3-OHKYN-13C215 N, KYN-D4, 3-OHAA-D3, TRP-D8, KA-D5, and AA-15 N all at 40 μM, QA-D3 at 81 μM and XA-D4 at 82 μM was prepared by aliquoting 15, 40, 60, 60, 39, 20, 24, 80, and 70 μL of the respective individual stocks and diluting to a final volume of 4.0 mL with TDI water. About 1.0 mL of each standard mixture A, mixture B, mixture C, mixture D, and working SIL mixture were aliquoted in multiple sets of five separate 1.5 mL Eppendorf tubes and stored at −20 °C. To avoid the freeze/thaw cycle, on the day of the experiment, a set of three vials (A, B, and SIL) or (C, D, and SIL) were first thawed at room temperature in the dark cabinet before using these vials to prepare a calibration curve for analysis. All the dilutions were performed in an ice bath and the dark under yellow light.

2.2.3. Preparation of calibrants for CSF study

Working standard mixtures, A and B (prepared in section 1.2.2) were separately diluted at eight different concentrations in 1.5 mL Eppendorf tubes with TDI water. The calibrant mixtures A1-A8 consisting of TRP, 3-OHKYN, 3-OHAA, and XA (2, 7, 27, 100, 376, 1411, 5290, and 19837 nmol L^{-1}), KYN (2, 7, 27, 101, 379, 1420, 5325, and 19969 nmol L^{-1}), AA (2, 7, 27, 102, 381, 1430, 5360, and 20102 nmol/L), KA (1.6, 6, 23, 87, 326, 1223, 4585, and 17192 nmol L^{-1}) were prepared by serial dilution of standard mixture A. The calibrant mixtures B1–B8 consisting of PA (7, 16, 36, 80, 178, 399, 893, and 2000 nmol L^{-1}), and QA (7, 16, 36, 81, 180, 404, 904, and 2023 nmol L^{-1}) were all prepared separately serial dilution of standard mixture B. The SIL mixture A1 was prepared at the following concentrations: QA-D3 and XA-D4 2 μmol L^{-1}, PA-D4, 3-OHKYN-13C215 N, L-KYN-D4, 3-OHAA-D3, TRP-D8, KA-D5, and AA-15 N 1 μmol L^{-1} by aliquoting 25 μL of the working SIL mixture (prepared in section 1.2.2) and diluting at a final volume of 1.025 mL with TDI water. A separate SIL mixture A2 was prepared (for analysis of quality control samples) at the following concentrations: QA-D3 and XA-D4 4 μmol L^{-1}, PA-D4, 3-OHKYN-13C215 N, L-KYN-D4, 3-OHAA-D3, TRP-D8, KA-D5, and AA-15 N 2 μmol L^{-1} by aliquoting 75 μL of the working SIL mixture (prepared in section 1.2.2) and diluting to a final volume of 1.5 mL with TDI water.

The eight calibration vials were prepared by adding 100 μL of calibrant mixture A1-A8, 100 μL of calibrant mixture B1–B8, and 200 μL of SIL mixture A1 in eight separate 1.5 mL Eppendorf tubes and vortexing for 10s. About 150 μL samples were transferred to HPLC vials with micro inserts for injections.

2.2.4. Preparation of calibrants for plasma study

Working standard mixtures C and D (prepared in section 1.2.2) were separately diluted at eight different concentrations in 1.5 mL Eppendorf tubes with TDI water. The calibrant mixtures C1–C8 consisting of PA, KA, and AA (2, 5, 13, 36, 101, 284, and 800 nmol L^{-1}), 3-OHAA (1.6, 4, 12, 35, 98, 277, and 780 nmol L^{-1}), QA (4, 13, 38, 113, 337, 1005, and 3000 nmol/L), 3-OHKYN (4, 10, 29, 81, 227, 639, and 1800 nmol L^{-1}), XA (15, 42, 119, 336, 945, 2663, and 7500 nmol L^{-1}), KYN (45, 127, 358, 1009, 2843, 8009, and 22560 nmol L^{-1}) all prepared by serial dilution of standard mixture C. The calibrant mixtures D1-D8 consisting of TRP (15, 21, 30, 42, 60, 85, and 120 μmol L^{-1}) were prepared by serial dilution of working standard mixture D separately in TDI water. The SIL mixture B1 was prepared at the following concentrations: QA-D3 and XA-D4 1.25 μmol L^{-1}, PA-D4, 3-OHKYN-13C215 N, L-KYN-D4, 3-OHAA-D3, TRP-D8, KA-D5, and AA-15 N 0.6 μmol L^{-1} by aliquoting 55 μL of the working SIL mixture and diluting to a final volume of 3.6 mL with TDI water. The SIL mixture B2 was prepared at the following concentrations: QA-D3 and XA-D4 2.5 μmol L^{-1}, PA-D4, 3-OHKYN-13C215 N, L-KYN-D4, 3-OHAA-D3, TRP-D8, KA-D5, and AA-15 N 1.2 μmol L^{-1} by aliquoting 31 μL of the working I.S. mixture (prepared in section 1.2.2) and diluting to a final volume of 1.015 mL with TDI water. The eight calibration vials were prepared by adding 50 μL calibrant mixture C1–C8, 50 μL calibrant mixture D1-D8, and 50 μL SIL mixture B1 in eight separate 1.5 mL Eppendorf tubes and vortexing for 10s. The entire volume from each vial was transferred to the HPLC vial with micro inserts for the injections.

2.2.5. Preparation of CSF and plasma samples

All procedures involving the human subjects from Emory University

were a priori approved by the Emory Institutional Review Board, and all subjects recruited at Emory University provided written informed consent. The human plasma (a total of 34 samples, of which 2 samples were collected from each patient at a 1–3 h gap) and CSF (a total of 17 samples) analyzed for KP metabolites were obtained as blinded to the clinical status of study participants.

The CSF samples stored at −80 0C were first thawed at room temperature in a dark cabinet for approximately 30 min. Unknown (patient) CSF samples were prepared by adding 60 μL of SIL mixture A1 containing nine deuterated KP compounds (at variable concentrations) to 60 μL of human CSF in a 1.5 mL Eppendorf tube. To validate the precision and accuracy of the method, the quality control (QC) CSF samples were randomly selected from only one human subject vial with enough CSF material. The QC samples were prepared by the standard addition method by aliquoting 15 μL of calibrant mixture A (containing PA and QA), 15 μL of calibrant mixture B (containing 3-OHKYN, KYN, 3-OHAA, TRP, XA, KA, and AA), of low, medium, and high concentrations, and 30 μL of SIL mixture A2 (2X concentration of SIL-IS mixture A1) added to the 60 μL of human CSF in1.5 mL Eppendorf tube. Both unknown CSF samples and QC samples were vortexed for 15 s, and 20 μL was injected into the LC-MS/MS instrument.

A commercial healthy plasma sample (entire lyophilized powder) was mixed with 5 mL of TDI water by vortexing for 30 s and stored at −80 0C. Patient plasma samples stored at −80 0C were thawed at room temperature in a dark cabinet for approximately 30 min. Three QC plasma samples were prepared from the commercial lyophilized (powder) form of plasma. The patient plasma and QC plasma samples were prepared in four steps by solid-liquid extraction (SPE) using a PhreeTM phospholipid removal cartridge. First, 300 μL of ACN containing 1% FA was added to the cartridge, and 100 μL of unknown plasma sample was added on top of ACN in the cartridge. Second, 50 μL of SIL-IS mixture B1 was added to the cartridge and vortexed for 5 min to support mixing and protein precipitation. Third, the cartridge was attached to the SPE apparatus, and the liquid containing target analytes was eluted by applying ~10 in Hg vacuum, collected in a 1.5 mL Eppendorf tube, and dried for several hours with nitrogen in the SPE chamber. The QC plasma samples were prepared by aliquoting 100 μL of commercial plasma, adding 12.5 μL of each calibrant standard mixtures C and D (composition described in supplementary section) of low, medium, and high concentrations, and 25 μL of SIL-IS mixture B2 (2X concentration of SIL-IS mixture B1). Next, the QC plasma solution was added directly into the SPE cartridge containing 300 μL of ACN, 1% (v/v) FA. The steps for preparing QC plasma samples were similar to the patient plasma mentioned above. Dried patient and QC plasma samples were reconstituted in 100 μL TDI H2O and then transferred to micro insert LC vial for LC-MS/MS injection. The QC samples were injected between calibration injections and unknown patient samples **1.3. LC-MS/MS instrumentation**.

LC-MS/MS analysis was carried out on Agilent 1100 series HPLC system equipped with a binary pump (including degasser), thermostatted autosampler, and a temperature-controlled column compartment. Experiments with microbore C-18 column were carried out on Agilent 1200 series capillary HPLC system equipped with a binary pump, degasser, and a thermostatted autosampler. All four columns [Poroshell EC C-18, 1 mm × 75 mm, 2.7 μm; ZORBAX Eclipse-XDB C-8, 3.0 mm × 150 mm, 5 μm; Poroshell 120 Phenyl-Hexyl, 2.1 mm × 150 mm, 2.7 μm, and Poroshell 120 HILIC-Z, 2.1 mm × 150 mm, 2.7 μm] for stationary phase screening were obtained from Agilent Technologies, Inc (Santa Clara, CA, USA). Method validation was carried out on a C-8 reversed-phase analytical column using optimized mobile phase [A (0.2% (v/v) formic acid in acetonitrile/H_2O (1: 99 v/v)) and B (0.2% formic acid in MeOH)]. Optimum separation was achieved by using linear gradient elution with 5% B to 46.25% B from 0 to 11 min (3.75 % B/min) followed by post-conditioning for 5 min to reach the initial 5%B. The flow rate was 0.6 mL min^{-1}, and the column was operated at ambient temperature. Agilent 6410 triple quadrupole mass spectrometer was used with ESI in positive ion multiple reaction monitoring (MRM) mode. The MRM parameters for quantifier and qualifier, mass transitions, and dynamic multiple reaction monitoring (dMRM) are listed in Table S1-SII.

2.3. Method validation

The method was validated for selectivity, linearity, carryover, LOD, LOQ, precision, accuracy, matrix effect, and freeze-thaw stability according to FDA US Food and Drug Administration (FDA) guidelines [22]. SIL.

2.3.1. Sensitivity, and linearity

The sensitivity of the analytical method was determined by the instrument limit of detection (ILOD), and the LOQ was estimated at a *S/N* of 10. The ILOD was calculated from the %RSD of the measured area response of the replicate injections and the statistical confidence factor t. The ILOD is presented as t (99% CL) × % RSD × concentration of the injected standard (close to the expected calculated limit of detection (CLOD), see example calculation in supplementary section). The linearity was evaluated from R^2 values obtained from the standard curve calculated by the ordinary least square linear regression method. The standard curve was prepared using the internal standard method (aka. SIL).

2.3.2. Precision, accuracy, and matrix effects

Precision and accuracy were determined using QC samples prepared by spiking CSF and plasma samples at three different concentrations (low, medium, and high). Accuracy was assessed by percent recovery (100 x [Average concentration of endogenous analyte in unspiked sample + known concentration of added standard.]/Measured (found) concentration of analytes in spiked sample). The precision was expressed as % RSD. The matrix effect (ME) was evaluated from the peak area of SIL prepared in TDI water (neat blank), and the SIL spiked in one representative CSF or plasma. The percent ME was determined as 100 x (1- [peak area of spiked SIL in human CSF or plasma samples/peak area of SIL in the neat blank]).

2.3.3. Carryover and stability assessment

The carryover effect is the presence of any residual peak when a blank is injected after analyte/sample injection at high concentrations. In the present study, the carryover effect was determined by injecting a solvent blank (water) immediately after the injections of a calibrant mixture of the highest standard concentrations. The percent carryover was presented as 100 x (peak area of analyte in blank injection/peak area of analyte in highest concentration calibrant injection). A change in the peak area determined the stability of nine KP analytes standards and SILs. The stock solutions were stored in the autosampler tray at 4 °C for 21 h, and the peak areas of standards and SIL were compared at time zero and after 21 h. Changes in endogenous concentration determined the stability of the endogenous analytes in CSF during repeated freeze/thaw (F/T) cycles. The F/T stability was evaluated for five cycles and presented as (100 – [peak area ratio (endogenous analyte/SIL) from 1st F/T cycle - peak area ratio (endogenous analyte/SIL) from nth F/T cycle]/peak area ratio (endogenous analyte/SIL) from nth F/T cycle) x 100; n = 1, 2, 3, 4, and 5.

2.3.4. Data analysis

All data, including qualitative and quantitative analysis, were collected using the Agilent Mass Hunter data acquisition software version B.08.00. The peak areas of extracted ion chromatograms (EIC) for each MRM mass transition were integrated using the Agile-2 algorithm provided in the analysis software.

2.3.5. Statistical analysis

Statistical analysis includes a two-tailed Student's t-test or paired *t*-

test, and Pearson correlation (r) was performed with Microsoft Excel. P values < 0.05 were considered statistically significant [23]. The data were transformed to log as needed to approximate the linearity before calculating r. The Pearson correlation coefficient $0.3 < r < 0.7$ indicated moderate, $r \geq 0.8$ indicated strong and $r < 0.3$ indicated weak or no correlation between two variables. The t-score of correlation coefficient (r) was calculated as $t = r\sqrt{((n-2))}/\sqrt{((1-r^2))}$ (n = sample size). The p-value for Pearson correlation was calculated from t-distribution and degree of freedom.

3. Results and discussion

Simultaneous separation of all eight TRP metabolites in a single run is challenging because five metabolites (PA, QA, 3-OHAA, XA, KA, and AA) are hydrophobic with positive log P (0.2–1.3) [24], and only three of the metabolites (3-OHKYN, KYN, and TRP) are hydrophilic with negative log P (−1.1 to −2.5) [24]. Additionally, the different polarity, the extent of ionization, and functional groups among KP compounds (see chemical structures in Fig. S1) result in differential chromatographic and marked differences in endogenous levels. For example, due to the presence of single or multiple carboxyl groups (pKa = 1.0–3.5) in the structure of KPMs, their retention factor in the mobile phase higher than pH 4 is very small decreasing metabolite selectivity, requiring the need for post-column derivatization combined with column switching [25]. Furthermore, healthy subjects' endogenous plasma TRP levels are in the mid-micromolar range (40–90 μM) [5]. In contrast, baseline concentrations of QA in plasma are usually in the low nanomolar range (300–898 nM) [15,16] and even lower in CSF (12–898 nM) [15]. This information based on the above discussion indicates a need to separate KP metabolites in the low pH range and quantitate several KP analytes at lower sensitivity while maintaining high sensitivity for others.

3.1. MRM and spray chamber parameters optimization

Before evaluating the performance of the proposed method for the simultaneous assay of multiple KP metabolites, we optimized ESI-MS/MS conditions that may affect detection sensitivity. Due to the different endogenous levels of KPMs, specific mass spectrometer parameters must be optimized for each compound to provide the best performance. Flow injection with direct infusion was carried out to optimize the MRM parameters of each metabolite. A 20 μL of the KP compounds were injected at concentrations of 1–5 μM in 50:50 MeOH/H2O into the LC-MS/MS without column. The mobile phase containing 0.1% FA in 50:50 MeOH/H2O was used for the optimization. The optimized MRM mass transitions, fragmentor voltage, and collision energy of nine KP metabolites and nine SIL are summarized in Tables S–1 of the Supporting Information. The TRP and its eight metabolites provide superior sensitivity (49,000 to 333,882) peak abundances in the positive ion ESI-MS/MS even for those metabolites (QA, PA, KA, and XA) with carboxylic functional groups and without primary amine function. We attempted to optimize the most sensitive transition from precursor ion to product ion of tryptophan and eight of its metabolites along with the SIL of each metabolite. Transitions with the most abundant product ions were selected as a quantifier for quantitative analysis, while the second most abundant product ions were selected as a qualifier to confirm the identity of each KP analyte in CSF and plasma samples. Spray chamber parameters were fine-tuned using QA as a model test analyte to maximize *S/N*. Fig. S2 shows that S/N was optimum at a nebulizer pressure of 50 psi, drying gas flow rate of 12 L min^{-1}, drying gas temperature of 350 °C, and ESI voltage of 3000 V.

3.2. Dynamic multiple reaction monitoring (dMRM)

When monitoring many mass transitions in MRM mode, sensitivity and data quality can be compromised due to insufficient data points collection. The dynamic multiple reaction monitoring (dMRM) modes on a triple quadrupole MS allow one to monitor each mass transition only during a predetermined time window (delta retention time). Thus, MS cycle time (time required for the acquisition of all transitions) is reduced, and the dwell time (time needed for the acquisition of a single transition) is increased, resulting in a uniform and adequate number of data points across the peak. For accurate and precise quantitation of nine KP analytes, the dMRM method was developed using the retention times obtained with the final optimum experimental conditions. The delta retention time of 2 min was found to have a sufficient baseline of 1 min before and after the elution of each peak. The retention time repeatability of the developed method allowed the selection of narrow retention time windows (Tables S–2), enabling sensitive analysis of KPMs with better LODs.

3.3. Screening of stationary phases

Four stationary phases (C-18, C-8, Phenyl-Hexyl, and HILIC) were evaluated for simultaneous separation of TRP and its eight metabolites (Fig. 1). Based on the optimized gradient, a ternary mobile phase of ACN/MeOH/H_2O (conditions stated in Fig. 1) using the C18 core-shell stationary phase of 10% carbon loading, 2.7 μm particle size provided significant retention and separation of six out of nine KP analytes. The PA eluted closed to the unretained time of uracil, but QA and 3-OHKYN remain unresolved (Fig. 1A). On the other hand, on a standard (porous) C-8 phase with similar carbon loading of 7.6% but with a larger particle

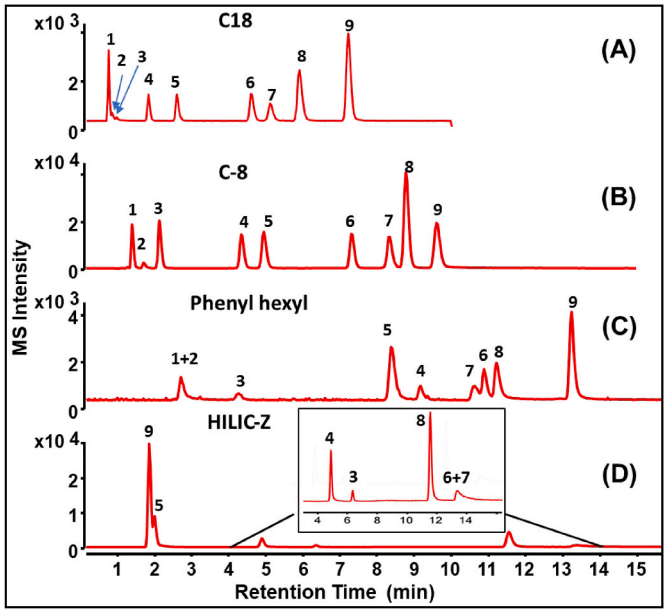

Fig. 1. Optimization of stationary phase for simultaneous separation of KP metabolites. **(A)** MP A: 0.1% FA in 1% ACN/4% MeOH/95% H2O; MP B: 0.1% FA in ACN; Separation conditions: Initial isocratic hold is 1 min at 5% B followed by 5% B to 40.5% B from 1 to 10 min; (gradient time (tg) = 3.94 %B/min). Post time was set to 10 min. Flow rate: 75 μL min-*1; Inj.*: 1 μL*; Analytes: 2*–3 μM *(in 100% H2O). **(B)** MP A: 0.2% FA in 99% H2O, 1% ACN; MP B 0.2% FA in MeOH, Separation conditions: 5% B to 61.25% B from 0*-11 min *(tg = 5.6% B/min) post time was set to* 5 min*, Flow: 0.6 mL min-1; Inj.*: 10 μL*; Analytes: 1*–2 μM *(in 100% H2O). **(C)** MP A: 0.1% FA in H2O; MP B: 0.1% FA in ACN, Separation conditions: gradient 1.4% B to 10%B from 0-*2 min *followed by 10% B to 56% B from 2-*15 min *(tg = 4.2%B/min) post time was set to* 10 min*, Flow: 0.2 mL min-1; Inj.*: 1 μL*; Analytes*: ~ *2*–3 μM *(in 100% H2O). **(D)** MP A: 0.1% FA in ACN, MP B: 0.1% FA in H2O; separation conditions: Hold 10% B for* 2 min *followed by 10% B to 60.5% B from 2-*15 min *(tg = 3.9%B/min), post time was set to* 10 min*; Flow: 0.3 mL min-1; Inj.*: 1 μL*; Analytes: 2*–3 μM *(in 100% H2O). MS conditions: Nebulizer pressure: 50 psi, DGF: 12 L min-1, DGT: 350°C, ESI voltage: 3000 V. Peak identifications: (1) PA, (2) QA, (3) 3-OHKYN, (4) KYN, (5) 3-OHAA, (6) TRP, (7) XA, (8) KA, and (9) AA.*

size of 5 μm provided considerable retention of PA, QA, and 3-OHKYN, resulting in simultaneous separation of all nine KP analytes in 10 min using an optimized ternary gradient with a slightly higher gradient rate compared to the C18 phase. (Fig. 1B). Additionally, on a C-8 phase, switching solvent B from ACN to MeOH improved the separation of later eluting peaks, and the use of 1% ACN in solvent A containing H_2O, provided a smooth baseline around earlier peaks (PA, QA, and 3-OHKYN) which was initially noisy when solvent A contained only H_2O. One would expect the use of a C-18 core-shell column of a longer length of 150 mm to be more effective than the 75 mm length that we have used in this work. However, operating with a 150 mm long C-18 column at 75 μL/min was very close to the 400-bar pressure limit on the Agilent G1376A pump. We observed the same column back pressure issue with the C-8 core-shell column of 150 mm length and 1 mm i.d, but not with HILIC and Phenyl-Hexyl stationary phases which were available at larger i.d of 2.1 mm. Hence, the latter two commercially available stationary phases, were evaluated with the hope of improving the retention and resolution of PA and QA. Under the respective optimized gradient conditions, the Phenyl-Hexyl phase (Fig. 1C) still could not resolve PA/QA pair. However, seven out of nine KP analytes were resolved with a much longer analysis time of 14 min. As expected, AA (the most retained KPM in the three hydrophobic phases) was the first to elute in the HILIC phase, but the elution order of the remaining KPM was not exactly reversed in this phase compared to the other three hydrophobic phases. Furthermore, the repeatability of separation was unreliable with poor resolution and peak shapes in the HILIC phase. Due to the strong adsorptive properties of the HILIC phase, the MS signal intensity of the last eluting KPM, such as the TRP/XA peak pair, was so broad that it was hard to distinguish from the baseline, and no peaks were seen even in the EIC mode for PA and QA. The plate count (plates/m) on all four stationary phases is tabulated in Tables S–3. Two important trends are worth mentioning. First, note that the average plates/m for all KPM was always higher on a C-8 phase compared to a C-18 phase. Second, the Phenyl-Hexyl and HILIC phases provided similar or higher plate count (compared to C-8 phase) for all KPM except PA and QA which were not retained in these two phases.

Although hydrophobicity is the dominant retention mechanism on reversed phase C18, C8, and phenylcolumns, the selectivity trends of KPM suggest that it is strongly influenced by several other parameters such as cation selectivity, and hydrogen bond donating and accepting capacity, π-π interactions as well as steric hindrance. First, note that both PA and QA have possible cation-exchange selectivity, but these interactions are reduced at the low pH of the mobile phase. Even though log P (0.2) of QA is less than PA (0.8), the relatively higher retention of QA could be due to the presence of more hydrogen bond donating and accepting carboxyl groups. Second, KYN and 3OH-KYN are less hydrophobic than PA and QA but are retained more in all three hydrophobic phases. This increased interaction can be attributed to the exposed (unreacted) silanol on the stationary phase that can donate protons to the basic (amines and amide groups) of KYN and 3OH-KYN. Third, the retention order of KYN/3-OHAA and TRP/XA metabolites pairs was reversed in the Phenyl-Hexyl phase compared to C18 and C8 phases. The former and latter reversal of the two metabolite pairs could be attributed to relatively more exposed silanol groups. Consequently, more hydrogen bonding and π-π interactions exist in the Phenyl-Hexyl phase. Finally, KA and AA are significantly more hydrophobic and are retained and eluted in the same order in all three hydrophobic phases. While only three out of nine KPMs are hydrophilic, RP stationary phases (Fig. 1A–C) were still more selective than the HILIC phase (Fig. 1D) for separating KP metabolites. Nevertheless, the fine-tuning of the stationary phase suggests that C-8 is the best phase for the simultaneous separation of nine KPM with good retention and resolution of highly charged and polar compounds such as PA and QA without excessive retention of hydrophobic KPMs (XA, KA, and AA).

3.4. Mobile phase optimization

Formic acid is a well-established additive for reversed-phase LC-MS as it provides a buffered mobile phase to stabilize retention time and generates protons by producing [M+H]+ions. Next, % (v/v) FA composition was optimized to achieve a shorter analysis time and maximize resolution between PA and QA but without significantly affecting the resolution of late eluting KPMs and excessive analysis time. Higher resolution between PA and QA is highly desired to avoid possible matrix interferences during quantitation in plasma and CSF samples. In Fig. 2A–D, we present overlaid chromatograms for separating nine KP compounds upon increasing the percent FA in the mobile phase from 0.1% to 0.6% (v/v). Increasing FA content, consistently improved resolution between PA and QA pair (i.e., 1/2 peak pair, inset Table). In contrast, KYN and 3-OHAA (i.e., 4/5 peak pair) coeluted at 0.4% (v/v) of FA. The resolution between XA/KA (i.e., 7/8 peak pair) deteriorated with an increase in percent FA. Furthermore, higher than 0.2% FA provides shorter run times, but AA ultimately merged with KA. Therefore, 0.2% FA was a good compromise because PA/QA was resolved more than baseline without significantly affecting the resolution of later eluting peak pairs.

The mobile phase flow rate was assessed at 0.4, 0.5, 0.6, 0.7-, and 0.8-mL min^{-1} (Figure S3, A-E). Increasing the flow rate from 0.4 mL min^{-1} to 0.8 mL min^{-1} reduced analysis time and increased the resolution of later eluting metabolites (KYN/3-OHAA and XA/KA pairs, inset Table, Fig. S3). The resolution of the PA/QA pair also improved until 0.6 mL min^{-1} but slightly deteriorated at flow rates of >0.7 mL min^{-1}. The flow rate of 0.6 mL min^{-1} was chosen to be the overall optimum based on the resolution of three critical peak pairs (see inset Table, Fig. S3), a good trade-off between resolution and total analysis time, as well as reduced solvent consumption.

3.5. Method validation

3.5.1. Selectivity

In an HPLC-MS/MS assay, endogenous KPM are susceptible to selectivity issues due to possible inference from isobaric compounds or structural analogs, which may be generated from the same biological pathway as the targeted analytes. However, it is very challenging to establish selectivity since the multiple KPMs are always present in the matrix. For example, chromatographic separation of PA from its endogenous structural analogs QA is critical, otherwise, their concentration will be overestimated since the above pair of KP compounds share the same product ions ($m/z = 78$ for PA and QA) in a tandem mass spectrometer (Table SI). Therefore, the selectivity was verified by the difference in retention times as shown in the EIC of PA/QA and all other KPMs in both CSF and plasma samples (Fig. 3 and S4). The selectivity of the method was examined by analyzing neat (water) blank (Fig. 3A and Fig. S4A), unspiked human CSF and plasma (Fig. 3B and Fig. S4B), CSF and plasma spiked with KP standards (Fig. 3C and Fig. S4C) and SILs (Fig.3D and Fig. S4D). As shown in Fig. 3A–D in CSF samples no direct interference was observed of any other substances at the retention time of each KP analyte. The EIC of PA for both spiked and unspiked plasma (column 1, Fig. 4A, and Fig. S4B) showed a well-resolved (later eluting crosstalk peak). This later peak was assumed to be originated from QA as this peak elutes at QA's retention time but shares the same product ion ($m/z = 78$) as PA. This peak was not seen in the EIC of PA spiked with SIL (column 1, Fig. S4C). Except for the EIC of QA in plasma (column 2, Fig. S4B), all EICs shown in the top and bottom panel (Figs. S4B–D), showed symmetrical peaks for other KPMs without any evidence of other peak interferences in the retention time of the KP standards and SILs.

3.5.2. Linearity and sensitivity

As mentioned earlier, one of the biggest challenges for KP metabolite quantitation originates from the endogenous nature of these

% FA	*Rs 1* (1 / 2)	*Rs 2* (4 / 5)	*Rs 3* (7 / 8)
0.1	1.5 ± 0.0	5.2 ± 0.6	2.3 ± 0.1
0.2	2.2 ± 0.0	2.9 ± 0.1	1.9 ± 0.1
0.4	2.5 ± 0.1	0.0 ± 0.0	1.7 ± 0.0
0.6	2.8 ± 0.2	0 ± 0	1.7 ± 0.0

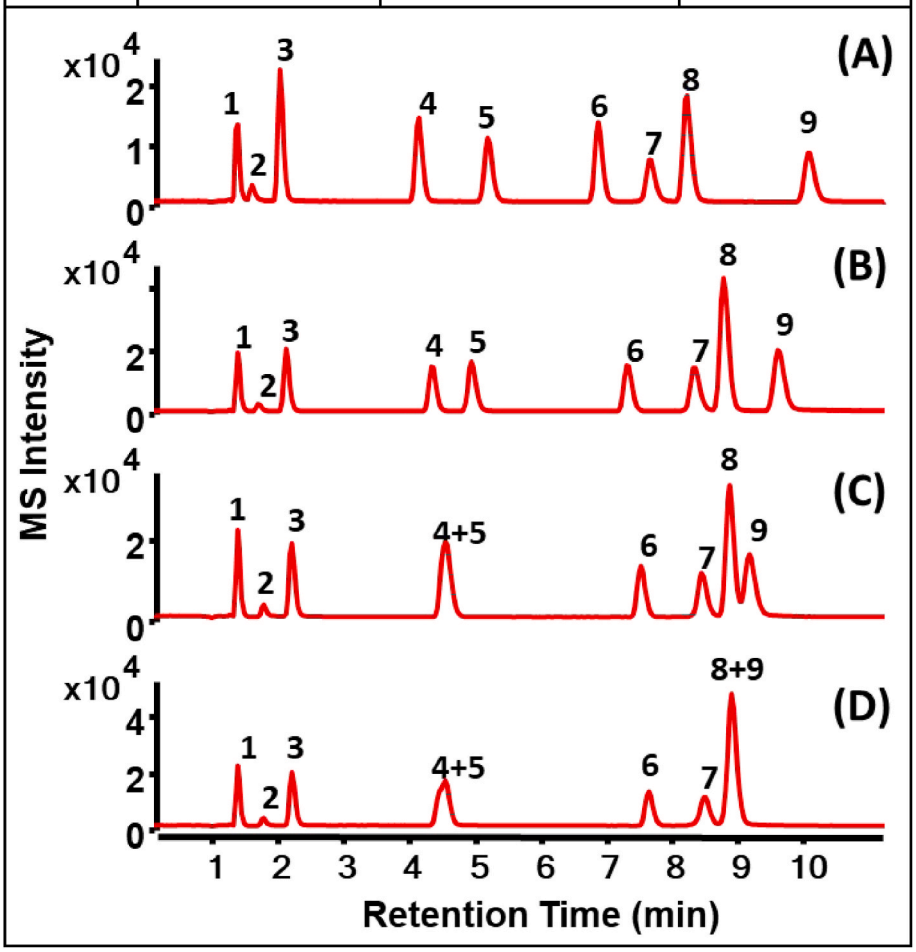

Fig. 2. Effect of formic acid content in mobile phase on separation of KP metabolites. **(A)** 0.1% FA, **(B)** 0.2% FA, **(C)** 0.4% FA, **(D)** 0.6% FA. Other experimental conditions are same as Fig. 1 B.

metabolites. Precise control blank matrix, without the presence of the KP, is unavailable. Therefore, in this study, we used a surrogate analyte approach using SILs. The eight-point calibration curves were constructed using peak area ratios of KPMs standards and SIL on the y-axis vs. concentration of KPMs on the x-axis. Standard solutions for all KP analytes and SILs were prepared in TDI water separately for both CSF and plasma to determine the concentration of KPMs from the slope of the calibration curve in these two biospecimens (Figs. S5 and S6). Excellent linearity was observed for all nine KP metabolites in CSF and plasma. The R^2 values were in the range of 0.9963–0.9999 for the calibration ranges used for CSF and 0.9977–0.9999 for plasma sample quantitation (Table-I, column 2). The developed method was highly sensitive for all nine KP metabolites with an ILOD in the range of 13–170 pM (pM) (Table-I, column 3). The LOQ is the lowest concentration in the standard curve that can be quantitated at a $S/N = 10$ and ranges between 0.07-0.80 nM and 0.08–1.801 nM in plasma and CSF, respectively (Table-I, column 4).

3.5.3. *Accuracy, precision, and matrix effect*

Accuracy and precision were evaluated using human CSF and commercial plasma samples spiked at three concentrations within the calibration range for all eight KPMs, including TRP. The accuracy of most of the metabolites in spiked CSF samples was within 80–120%, except for KA at the low spike concentration, which was 129% (Table-1, column 10, row 10). The precision of the determined concentration was $\leq$4% RSD except for XA, which was 12% at low spike concentration in CSF (Table 1, column 13, row 9). The ME in CSF samples was below the 15% acceptable limit except for PA (27%) and QA (16%) (Table-1, column 6, rows 3 and 4). The accuracy of all the KP metabolites in spiked plasma was between 84 and 118%, except 3-OHKYN at medium spike

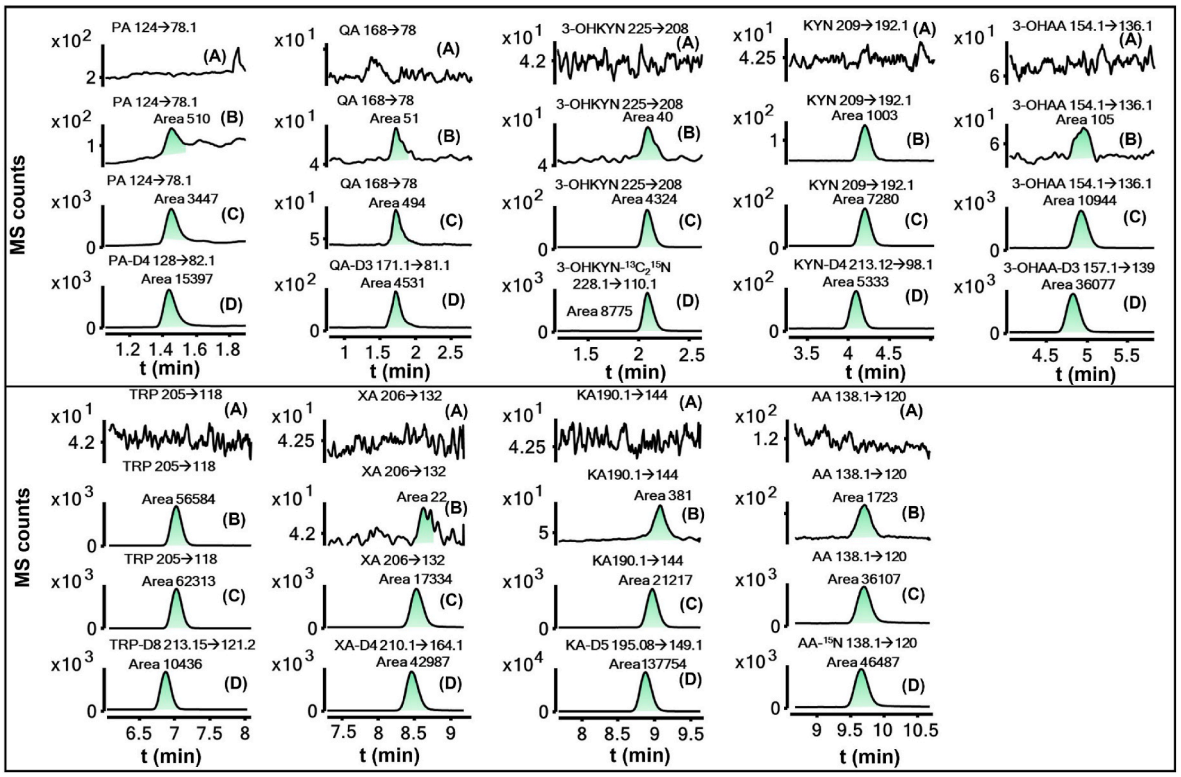

Fig. 3. Selectivity of 9 target analytes in CSF (A) EIC of TDI water (B) EIC of endogenous KPMs in human CSF, and (C) EIC of endogenous KPMs in CSF spiked with KPM standards, and (D) EIC of SIL spiked in CSF.

Table 1
Method validation for KPMs in human CSF and plasma.

Target Analytes	Linearity (R^2)	ILOD (nM)	LOQ (nM)	Calibration range (nM)	% ME	Spike levels			Accuracy (% Recovery)			precision (%RSD)		
CSF						Low	Med	High	Low	Med	High	Low	Med	High
PA	0.9968	0.15	1.4	3.5–1000	27	4	45	506	118	118	107	4	2	1
QA	0.9985	0.05	0.23	3.6–1011	16	4	45	500	81.0	108	100	0.6	1	1
3-OHKYN	0.9999	0.013	0.38	1–9919	4	1.8	94	4959	107	101	102	1	1	1
KYN	0.9998	0.17	0.21	1–9985	4	1.8	95	4992	115	105.23	103	1	0.01	1
3-OHAA	0.9999	0.17	0.21	1–9919	7	1.8	94	4959	84	101	104.1	3	1	0.5
TRP	0.9999	0.12	0.19	1–9919	4	1.8	94	4959	116.2	115.1	104.4	0.1	0.8	0.4
XA	0.9998	0.11	0.18	1–9919	4	1.8	94	4959	120	103	102.6	12	2	0.1
KA	0.9998	0.3	0.8	0.8–8596	4	1.5	82	4298	129	104.0	104.0	2	0.3	0.3
AA	0.9963	1.3	2.5	1–2680	1	1.8	95	5025	116.2	115	104.4	0.1	1	0.4
plasma						Low	Med	High	Low	Med	High	Low	Med	High
PA	0.9994	0.15	0.37	1.1–533	82	1.1	8.9	71	102	99	94	4	11	4
QA	0.9989	0.05	0.8	2.8–2000	11	3.2	28.2	251.3	107	98	100	7	5	3
3-OHKYN	0.9996	0.01	0.05	2.4–1200	−18	2.5	20.1	159.8	111	72	99	5	5	3
KYN	0.9998	0.17	0.43	30–1500	20	32	252	2002	99	96	113	1	2	1
3-OHAA	0.9998	0.17	0.26	1–520	19	1.1	8.7	69.2	109	96	84	1	8	3
TRP	0.9977	0.12	0.33	10–80[b]	−8	5.3	10.6	21.2	97	91	118	1	3	3
XA	0.9997	0.11	0.39	10–5000	−13	1.8	94	4959	[a]	[a]	[a]	[a]	[a]	[a]
KA	0.9999	0.04	0.07	1.1–533	−45	1.5	82	4298	[a]	[a]	[a]	[a]	[a]	[a]
AA	0.9990	0.25	0.1	1.1–533	1	1.1	8.9	71	92	108	101	2	3	1

[a] Not determined due to the unstable retention of XA and KA in plasma samples.
[b] TRP concentration in μM

concentration was 72% (Table 1, column 11, row 15). The precision was ≤5%RSD except for PA (11 %RSD), QA (7 %RSD), and 3-OHAA (8 % RSD) at medium, low, and medium spike concentrations respectively (Table-1, column 14-row 13, column 13-row 14, and column14-row 17). Accuracy and precision for XA and KA in the plasma samples were not determined since the retention time for both analytes was unstable. The ME was found to be significantly high for some of the KP metabolites in plasma samples except QA (11%), TRP (−8%), XA (−13%), and KA (1%) (Table-1, column 6, row 14, 18, 19, and 20). In the present study, SIL for all nine KP analytes was used to compensate for variations during all the sample preparation steps and matrix effects.

3.5.4. *Carryover and freeze-thaw stability*

No significant carryover was present for any of the KP metabolites. For example, the percent carryover for all the KP analytes was less than 5% of the peak area of the highest injected concentration of the

calibration curve. The stock solutions of standard KPMs and SILs were stable for 21 h at 4 °C (Tables S–4). Stocks of standards and SILs, stored at −22 °C did not significantly change after one F/T cycle. The percent change of peak area of standards after 21 h was less than 15%, except XA and KA were 17 and 18%, respectively (Tables S–4, column 2). The percent peak area changes for SILs were 1–2%, except PA-D4 was 10% (Tables S–4, column 5). After one F/T cycle, the percent change in the peak area of both standards and SILs was 1–9% (Tables S–4, columns 3 and 6).

The percent stability of endogenous KP analytes was determined in human CSF. All the endogenous analytes were stable throughout five repeated F/T cycles except for XA, which was not quantitated in the studied sample. The percent stability of KP analytes in CSF after the fifth F/T cycle was PA (93 ± 5), QA (93 ± 5), 3-OHKYN (95.7 ± 0.7), KYN (94 ± 4), 3-OHAA (92 ± 5), TRP (97 ± 4), KA (94 ± 2), and AA (102.2 ± 0.9) (Table-2, column 7). The endogenous levels of all the analyzed KP analytes were unaffected after four F/T cycles except for 3-OHAA, which fell to 90 ± 1 (Table 2, column 6, row 7).

3.6. KP metabolite concentrations in human CSF and plasma

All nine KP compounds were detected in the human CSF, and eight (except for XA) were successfully quantitated. Concentrations of XA in CSF were calculated to be outside (below) the LOQ in fourteen human subjects and below the lower limit of the calibration curve (i.e., 1 nM) in three subjects. Furthermore, in eight subjects, the concentration of 3-OHAA in CSF was below the lowest calibration point, and in two subjects, it was below the calculated LOQ. In human plasma, all nine KP metabolites were detected and quantitated successfully. XA and KA retention times were unstable in some of the plasma samples, making them unreliable for quantitation in a few samples. For this reason, the concentrations of XA and KA were determined only in twenty-three and thirteen plasma subjects, respectively, out of a total of 34 human subjects. Therefore, quantitative results of XA and KA in plasma and XA in CSF were not used for studying the association between the two body fluids and the regulation of low and high inflammation.

3.7. Association between CSF and plasma levels of KPMs in neuroinflammation

Recent evidence from human subject studies supports an interaction between several neuro-inflammatory disorders and the levels of KPMs in CSF and blood. Pearson's correlations statistical analysis was used to investigate the association of endogenous KP metabolite levels in human CSF versus plasma at two time periods (Table S-5 and Table S-6). The tabulated values for the mean CSF concentrations of KP metabolites and the corresponding concentrations in plasma collected at time t_1 and time t_2 showed positive or negative correlations. In particular, KYN and 3-OH KYN showed a stronger association between the two biofluids of human subject samples collected at time t_1. For example, mean CSF concentrations of 26 ± 9 nM of KYN ($r = 0.53$, $p = 0.080$) and 3-OHKYN 5 ± 4 nM ($r = 0.56$, $p = 0.047$) were moderately correlated with respective mean concentrations of 1070 ± 245 nM and 26 ± 8 nM, which is approximately 41 and 5 times higher in plasma than CSF (Fig. 4A). However, at time t_2, the mean CSF concentrations of at least four KP analytes (KYN, 3-OHKYN, 3-OHAA, and TRP) were significant [KYN ($r = 0.51$, $p = 0.037$), 3-OHKYN ($r = 0.53$, $p = 0.050$), TRP ($r = 0.52$, $p = 0.033$), and 3-OHAA ($r = 0.71$, $p = 0.032$)] (Fig. 4B). Notably, the above data indicate that 3-OHAA has the strongest association when CSF levels correlated with plasma. The CSF concentrations ratio of KYN/TRP ($r = 0.64$, $p = 0.010$) and ($r = 0.46$, $p = 0.066$) in plasma collected at both times, t_1 and t_2, respectively showed moderate but positive correlation with the concentration (Fig. 5A and B). Interestingly, 3-OHAA/AA showed moderate but negative correlation ($r = -0.49$, $p = 0.14$) at time t_1 (Fig. 5A) whereas strongly positive correlation ($r = 0.71$, $p = 0.021$) at time t_2 (Fig. 5B). Thus, a study with a higher sampling frequency could answer the two different trends. Two other pair of metabolites such as 3-OHAA/3-OHKYN ($r = 0.57$, $p = 0.085$) and PA/QA ($r = 0.44$, $p = 0.076$) concentrations in CSF showed moderately high but positive correlation with plasma collected at time t_1 (Fig. 5A) and t_2 (Fig. 5B) respectively. The supporting information section reported the Pearson's correlation plots of KPMs and the metabolite ratio that showed weak or no correlation (Figs. S7–S9). The mean plasma concentrations of all the analyzed KP metabolites were higher than in CSF, consistent with the reports on Huntington's disease [26], Alzheimer's disease [27], and depression [28].

3.8. Regulation of KP metabolites in low and high neuroinflammation

In the last decade, there has been growing evidence that an interaction exists between inflammation and the KP metabolite levels in depression. By generating box plots, mean CSF and plasma KP metabolites concentrations were compared in patients classified as subjects with low and high inflammation based on the test C-reactive protein (CRP) and the tumor necrosis factor (TNF-α). As shown in Fig. 6A (top left), QA was significantly upregulated in human plasma with high CRP ($p < 0.01$) but not in the plasma with high TNF-α ($p < 0.5$). On the other hand, plasma KYN was significantly upregulated in patients with both high CRP ($p < 0.05$) and TNF-α ($p < 0.005$) (Fig. 6 A, top right). Additionally, 3-OHKYN/KYN ratio (Fig. 6A, bottom left) in plasma was found to be significantly upregulated in high TNF- α ($p = 0.040$) subjects but found to be insignificant in high CRP ($p = 0.093$). The ratio of KYN/TRP in plasma was significantly upregulated in both high CRP ($p = 0.001$) and TNF-α ($p = 0.002$) (Fig. 6A, bottom right). The CSF KYN and TRP were significantly upregulated in TNF-α ($p = 0.005$ and $p = 0.019$, respectively) (Fig. 6B), but the ratio of the same two metabolites showed no correlation with CRP or TNF- α. (Fig. S10). The supporting information section reported the box plots of other CSF and plasma KP metabolites/ratios that were not significantly different between subjects classified under high and low inflammation (Figs. S10–S11).

4. Conclusions

A repeatable, selective, and sensitive reversed-phase HPLC-MS/MS method was developed for simultaneous separation and quantitation of nine KPMs using a commercial C-8 column and a ternary mobile phase

Table 2
Percent stability of KP metabolites in human CSF after one to five freeze-thaw cycles.

Analytes	Baseline Mean ± SD	‡% Stability				
		Thaw 1	Thaw 2	Thaw 3	Thaw 4	Thaw 5
PA	13 ± 2 nM	96 ± 0.1	96 ± 1	99 ± 1	101 ± 5	93 ± 5
QA	19 ± 4 nM	102 ± 1	104.3 ± 0.3	96 ± 2	97.7 ± 0.9	93 ± 5
3-OHKYN	5.7 ± 0.1 nM	94.2 ± 0.7	98 ± 4	95 ± 1	99 ± 1	95.7 ± 0.7
KYN	23 ± 6 nM	95.0 ± 0.7	98 ± 2	97 ± 4	98 ± 1	94 ± 4
3-OHAA	0.9 ± 0.1 nM	94 ± 4	100 ± 3	101 ± 3	90 ± 1	92 ± 5
TRP	1.07 ± 0.05 μM	99 ± 1	101 ± 3	101 ± 3	100 ± 3	97 ± 4
KA	0.12 ± 0.03 nM	96 ± 1	96 ± 9	99 ± 11	106 ± 10	94 ± 2
AA	1.4 ± 0.8 nM	104.5 ± 0.2	103.7 ± 0.4	103.4 ± 0.1	104.2 ± 0.2	102.2 ± 0.9

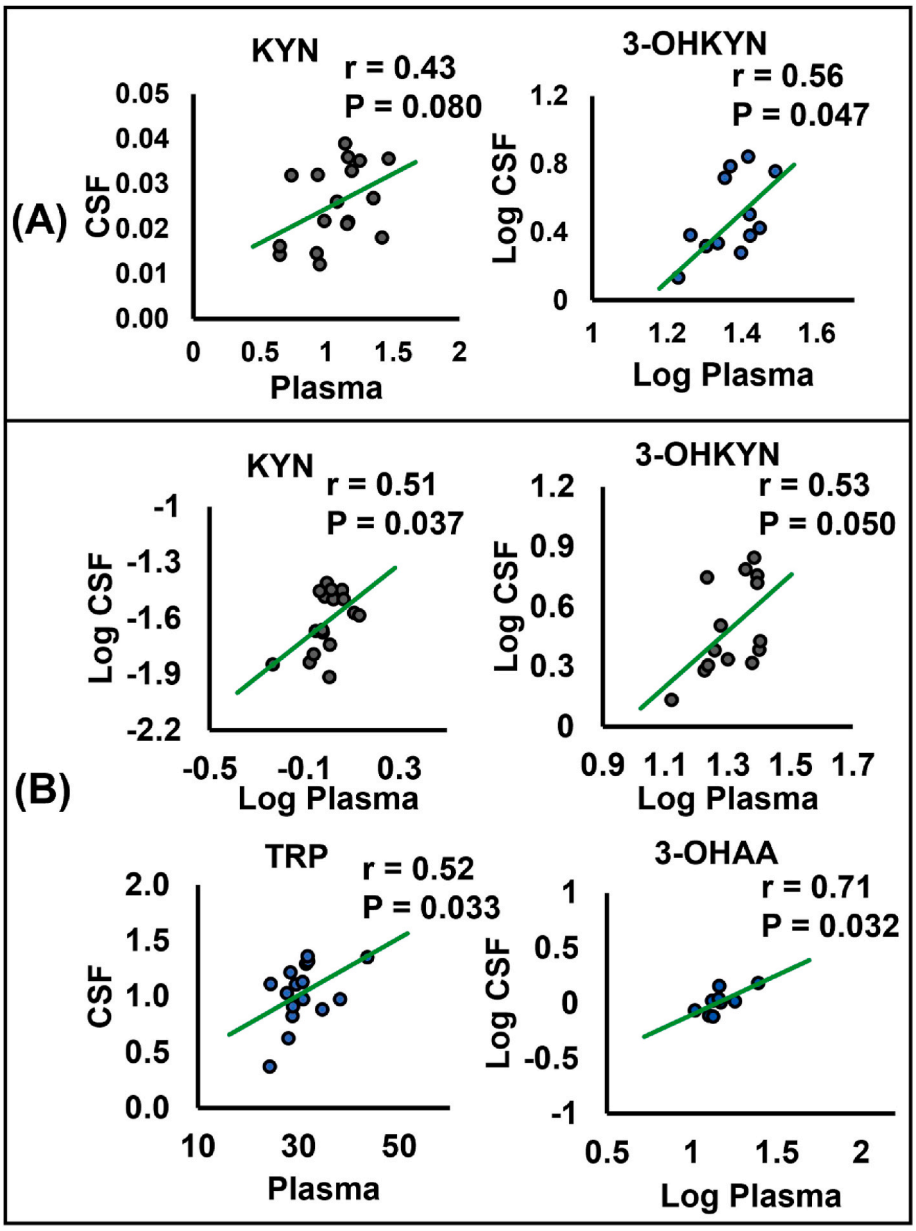

Fig. 4. Association of CSF and plasma KP metabolite concentrations in neuroinflammation patients. (A) plasma collected at time 1 and (B) plasma collected at time 2.

gradient from 5% (v/v) MeOH-95% (v/v) H_20-ACN (99:1) to 61.25% (v/v) MeOH-38.75% H_20-ACN (99:1) containing 0.2% FA at 0.6 mL min^{-1}. All nine KPMs were baseline separated for the first time in a single run within 10 min without any precolumn derivatization. The dynamic MRM methods on the tandem quadrupole instruments allowed us to tackle large multi-analyte KPM assays with high sensitivity. The developed method was satisfactorily validated for selectivity, sensitivity, linearity, precision, accuracy, matrix effects, carryover, and stability per US FDA guidelines. The calculated ILOD and LOQ for all nine KPMs were 0.013–0.25 nM and 0.08–1.4 nM in CSF and the range of 0.013–0.25 nM and 0.05–0.80 nM in plasma. Moreover, simultaneous linear calibration curves were established to measure the concentration of all KPMs in both human CSF and plasma. Evidence of KP involvement in living human depressed patients is limited. The average CSF and plasma levels of several KPMs (3-OHKYN, KYN, 3-OHAA, TRP as well as ratio of KYN/TRP and 3-OHAA/AA) were significantly associated, and the overall plasma levels (24 ± 7 nM, 1035 ± 214 nM, 16 ± 6 nM, 33 ± 5 μM, 0.032 ± 0.007 μM/μM, and 1.0 ± 0.7 nM/nM respectively) were higher than CSF (5 ± 4 nM, 26 ± 9 nM, 1.2 ± 0.5 nM, 1.0 ± 0.3 μM, 0.03 ± 0.01 μM/μM, and 0.19 ± 0.08 nM/nM respectively). The results align with previous reports on several other neurological disorders [26–28].

The ultimate goal of this optimized HPLC-MS/MS method was to determine the concentration of KP metabolites in the CSF and human plasma sample with low and high inflammation. The CSF and plasma level of KYN was significantly different and ranged from 23 ± 8 nM to 30 ± 9 nM in CSF and from 979 ± 235 nM to 1116 ± 151 nM in plasma in human subjects with low and high inflammation, respectively. as determined by TNF-α. However, for the same metabolite, the levels were not significantly different as determined by CRP. Similarly, TRP level was not significant in human plasma but significant in human CSF and ranged from 1144 + 155 nM to 1201 + 192 nM in low and high inflammation, respectively, for TNF-α. Conversely, the metabolite ratios of KYN/TRP and 3-OHKYN/KYN were significant in human plasma but not CSF. Finally, when comparing low and high inflammation (for CRP), the QA levels in human plasma were also significant and ranged from 57 + 13 nM and 78 + 24 nM, respectively. Nevertheless, this paper only followed a modest goal of providing quantifiable data on two biofluids. We found some evidence to support a substantial permutation of KP in

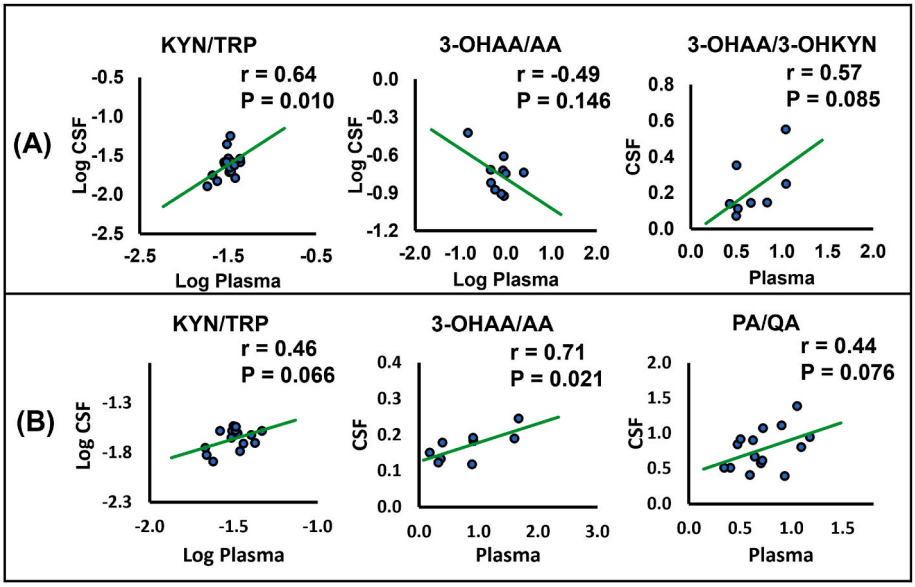

Fig. 5. Association of CSF and plasma KP metabolite concentrations ratio in neuroinflammation patients. (A) plasma collected at time 1 and (B) plasma collected at time 2.

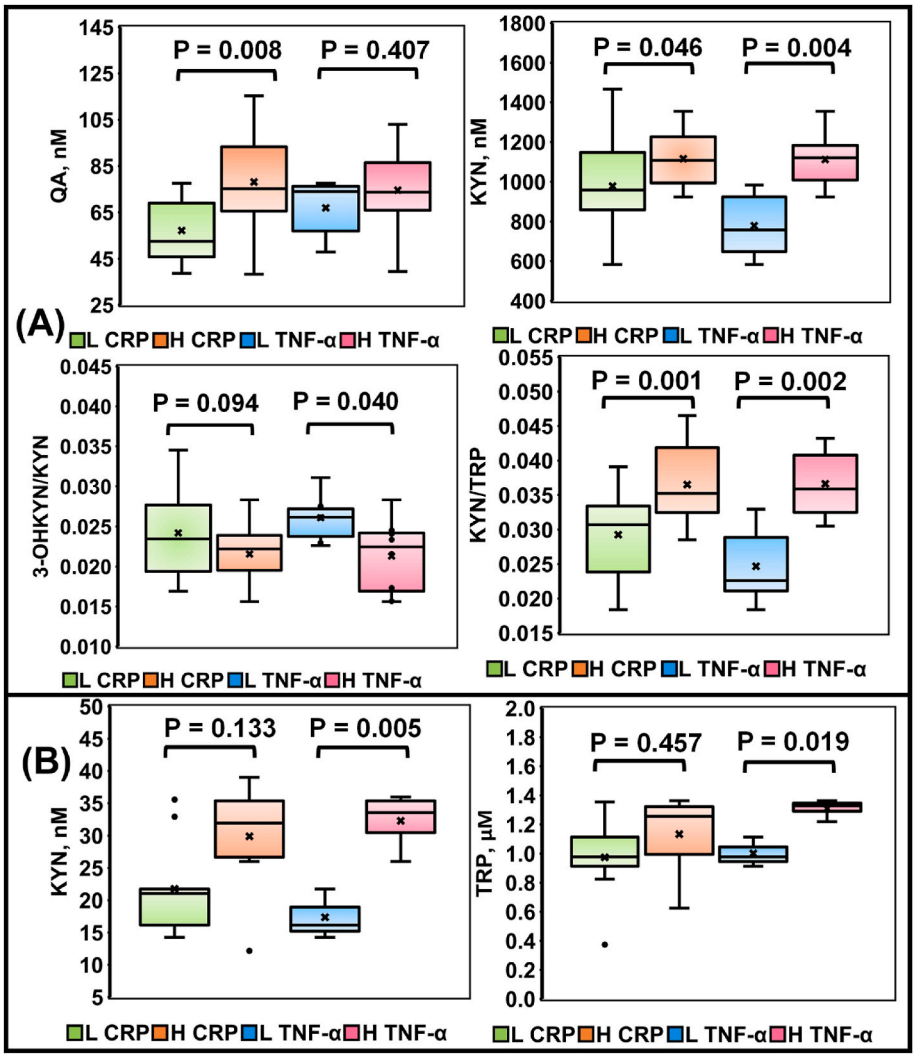

Fig. 6. Comparison of mean KP metabolite concentrations **(A)** of plasma and **(B)** of CSF in patients with low versus high CRP and low versus high TNF-a.

depression. Therefore, future studies are warranted to provide a detailed analysis of biofluid levels of neuroprotective and neurotoxic metabolites for a sizeable human subject population.

CRediT authorship contribution statement

Vijay D. Patel: Methodology, development, Data curation, Method, Validation. **Shahab A. Shamsi:** Supervision, Assistance, and Guidance in, Methodology, Validation, Funding acquisition. **Andrew Miller:** Human subject collection and initial screening of demographic. **Aimin Liu:** Visualization, Funding acquisition. **Mark Powell:** Assistance with column selections.

Declaration of competing interest

All the authors have declared that there was no competing conflict of interests that may have influenced the research data reported in this paper.

Data availability

No data was used for the research described in the article.

Acknowledgments

This project was financially supported by the National Institutes of Health (1 R21 MH107985–01).

Appendix A. Supplementary data

Supplementary data to this article can be found online at https://doi.org/10.1016/j.aca.2023.341659.

References

[1] P. Chatterjee, K. Goozee, C.K. Lim, I. James, K. Shen, K.R. Jacobs, H.R. Sohrabi, T. Shah, P.R. Asih, P. Dave, C. ManYan, K. Taddei, D.B. Lovejoy, R. Chung, G. J. Guillemin, R.N. Martins, Alterations in serum kynurenine pathway metabolites in individuals with high neocortical amyloid-β load: a pilot study, Sci. Rep. 8 (2018) 8008.

[2] K. Arnhard, F. Pitterl, B. Sperner-Unterweger, D. Fuchs, T. Koal, H. Oberacher, A validated liquid chromatography-high resolution-tandem mass spectrometry method for the simultaneous quantitation of tryptophan, kynurenine, kynurenic acid, and quinolinic acid in human plasma, Electrophoresis 39 (2018) 1171–1180.

[3] J. Quak, B. Doornbos, A.M. Roest, H.E. Duivis, N. Vogelzangs, W.A. Nolen, B.W.J. H. Penninx, I.P. Kema, P. de Jonge, Does tryptophan degradation along the kynurenine pathway mediate the association between pro-inflammatory immune activity and depressive symptoms? Psychoneuroendocrinology 45 (2014) 202–210.

[4] A.-M. Myint, Y.-K. Kim, Network beyond Ido in psychiatric disorders: revisiting neurodegeneration hypothesis, Prog. Neuro Psychopharmacol. Biol. Psychiatr. 48 (2014) 304–313.

[5] Y. Chen, G.J. Guillemin, Kynurenine pathway metabolites in humans: disease and healthy states, Int. J. Tryptophan Res. : IJTR 2 (2009) 1–19.

[6] H. Zuo, P.M. Ueland, A. Ulvik, S.J.P.M. Eussen, S.E. Vollset, O. Nygård, Ø. Midttun, D. Theofylaktopoulou, K. Meyer, G.S. Tell, Plasma biomarkers of inflammation, the kynurenine pathway, and risks of all-cause, cancer, and cardiovascular disease mortality: the Hordaland Health study, Am. J. Epidemiol. 183 (2016) 249–258.

[7] D.M. Christmas, J. Potokar, S.J. Davies, A biological pathway linking inflammation and depression: activation of indoleamine 2,3-dioxygenase, Neuropsychiatric Dis. Treat. 7 (2011) 431–439.

[8] M. Cihan, Ö. Doğan, C. Ceran Serdar, A. Altunçekiç Yıldırım, C. Kurt, M.A. Serdar, Kynurenine pathway in Coronavirus disease (COVID-19): potential role in prognosis, J. Clin. Lab. Anal. 36 (2022), e24257.

[9] L. Lionetto, M. Ulivieri, M. Capi, D. De Bernardini, F. Fazio, A. Petrucca, L. M. Pomes, O. De Luca, G. Gentile, B. Casolla, M. Curto, G. Salerno, S. Schillizzi, M. S. Torre, I. Santino, M. Rocco, P. Marchetti, A. Aceti, A. Ricci, R. Bonfini, F. Nicoletti, M. Simmaco, M. Borro, Increased kynurenine-to-tryptophan ratio in the serum of patients infected with SARS-CoV2: an observational cohort study, Biochim. Biophys. Acta (BBA) - Mol. Basis Dis. 1867 (2021), 166042.

[10] A. Sousa, C. Ribeiro, V.M.F. Gonçalves, J. Barbosa, B. Peixoto, A. Andrade, P. Silva, J.P. Andrade, S. Leal, Development and validation of a liquid chromatography method using UV/fluorescence detection for the quantitative determination of metabolites of the kynurenine pathway in human urine: application to patients with heart failure, J. Pharmaceut. Biomed. Anal. 198 (2021), 113997.

[11] S. Bourcier, J.-F. Benoist, F. Clerc, O. Rigal, M. Taghi, Y. Hoppilliard, Detection of 28 neurotransmitters and related compounds in biological fluids by liquid chromatography/tandem mass spectrometry, Rapid Commun. Mass Spectrom. 20 (2006) 1405–1421.

[12] F.M. Notarangelo, H.-Q. Wu, A. Macherone, D.R. Graham, R. Schwarcz, Gas chromatography/tandem mass spectrometry detection of extracellular kynurenine and related metabolites in normal and lesioned rat brain, Anal. Biochem. 421 (2012) 573–581.

[13] A.S.M.M.R. Chawdhury, S.A. Shamsi, A. Miller, A. Liu, Capillary electrochromatography-mass spectrometry of kynurenine pathway metabolites, J. Chromatogr. A 1651 (2021), 462294.

[14] L.-J. Hu, X.-F. Li, J.-Q. Hu, X.-J. Ni, H.-Y. Lu, J.-J. Wang, X.-N. Huang, C.-X. Lin, D.-W. Shang, Y.-G. Wen, A simple HPLC–MS/MS method for determination of tryptophan, kynurenine and kynurenic acid in human serum and its potential for monitoring antidepressant therapy, J. Anal. Toxicol. 41 (2017) 37–44.

[15] G.A. Smythe, A. Poljak, S. Bustamante, O. Braga, A. Maxwell, R. Grant, P. Sachdev, Ecni GC-MS analysis of picolinic and quinolinic acids and their amides in human plasma, CSF, and brain tissue, in: G. Allegri, C.V.L. Costa, E. Ragazzi, H. Steinhart, L. Varesio (Eds.), Developments in Tryptophan and Serotonin Metabolism, Springer US, Boston, MA, 2003, pp. 705–712.

[16] R. Vanholder, R. De Smet, G. Glorieux, A. Argilés, U. Baurmeister, P. Brunet, W. Clark, G. Cohen, P.P. De Deyn, R. Deppisch, B. Descamps-Latscha, T. Henle, A. Jörres, H.D. Lemke, Z.A. Massy, J. Passlick-Deetjen, M. Rodriguez, B. Stegmayr, P. Stenvinkel, C. Tetta, C. Wanner, W. Zidek, G. For the European Uremic Toxin Work, Review on uremic toxins: classification, concentration, and interindividual variability, Kidney Int. 63 (2003) 1934–1943.

[17] A. Meinitzer, A. Tomaschitz, S. Pilz, M. Truber, G. Zechner, M. Gaksch, B. Prietl, G. Treiber, M. Schwarz, A. Baranyi, Development of a liquid chromatography–mass spectrometry method for the determination of the neurotoxic quinolinic acid in human serum, Clin. Chim. Acta 436 (2014) 268–272.

[18] M. Möller, J.L. Du Preez, B.H. Harvey, Development and validation of a single analytical method for the determination of tryptophan, and its kynurenine metabolites in rat plasma, J. Chromatogr., B: Anal. Technol. Biomed. Life Sci. 898 (2012) 121–129.

[19] L. Orsatti, R. Speziale, M.V. Orsale, F. Caretti, M. Veneziano, M. Zini, E. Monteagudo, K. Lyons, M. Beconi, K. Chan, T. Herbst, L. Toledo-Sherman, I. Munoz-Sanjuan, F. Bonelli, C. Dominguez, A single-run liquid chromatography mass spectrometry method to quantify neuroactive kynurenine pathway metabolites in rat plasma, J. Pharmaceut. Biomed. Anal. 107 (2015) 426–431.

[20] F. Tömösi, G. Kecskeméti, E.K. Cseh, E. Szabó, C. Rajda, R. Kormány, Z. Szabó, L. Vécsei, T. Janáky, A validated UHPLC-MS method for tryptophan metabolites: application in the diagnosis of multiple sclerosis, J. Pharmaceut. Biomed. Anal. 185 (2020), 113246.

[21] L. Whiley, L.C. Nye, I. Grant, N. Andreas, K.E. Chappell, M.H. Sarafian, R. Misra, R. S. Plumb, M.R. Lewis, J.K. Nicholson, E. Holmes, J.R. Swann, I.D. Wilson, Ultrahigh-performance liquid chromatography tandem mass spectrometry with electrospray ionization quantification of tryptophan metabolites and markers of gut Health in serum and plasma—application to clinical and epidemiology cohorts, Anal. Chem. 91 (2019) 5207–5216.

[22] R. Meesters, S. Voswinkel, Bioanalytical method development and validation: from the USFDA 2001 to the USFDA 2018 guidance for industry, J Appl Bioanal 4 (2018) 67–73.

[23] D. Howitt, D. Cramer, Introduction to Research Methods in Psychology, third ed., Pearson Education Limited, Essex, England, 2011.

[24] R.S. Grant, S.E. Coggan, G.A. Smythe, The physiological action of picolinic acid in the human brain, Int. J. Tryptophan Res. 2 (2009) 71–79.

[25] S. Mitsuhashi, T. Fukushima, M. Tomiya, T. Santa, K. Imai, T. Toyo'oka, Determination of kynurenine levels in rat plasma by high-performance liquid chromatography with pre-column fluorescence derivatization, Anal. Chim. Acta 584 (2007) 315–321.

[26] F.B. Rodrigues, L.M. Byrne, A.J. Lowe, R. Tortelli, M. Heins, G. Flik, E.B. Johnson, E. De Vita, R.I. Scahill, F. Giorgini, E.J. Wild, Kynurenine pathway metabolites in cerebrospinal fluid and blood as potential biomarkers in Huntington's disease, J. Neurochem. 158 (2021) 539–553.

[27] K.R. Jacobs, C.K. Lim, K. Blennow, H. Zetterberg, P. Chatterjee, R.N. Martins, B. J. Brew, G.J. Guillemin, D.B. Lovejoy, Correlation between plasma and CSF concentrations of kynurenine pathway metabolites in Alzheimer's disease and relationship to amyloid-β and tau, Neurobiol. Aging 80 (2019) 11–20.

[28] E. Haroon, J.R. Welle, B.J. Woolwine, D.R. Goldsmith, W. Baer, T. Patel, J. C. Felger, A.H. Miller, Associations among peripheral and central kynurenine pathway metabolites and inflammation in depression, Neuropsychopharmacology 45 (2020) 998–1007.